

Online Monitor Against Clock and Orbit Ephemeris Faults in ARAIM

Mathieu Joerger, Yawei Zhai, Boris Pervan
Illinois Institute of Technology

BIOGRAPHIES

Dr. Mathieu Joerger obtained a Diplôme d'Ingénieur in Mechatronics from the Ecole Nationale Supérieure des Arts et Industries de Strasbourg, France, in 2002, and a M.S. and a Ph.D. in Mechanical and Aerospace Engineering from the Illinois Institute of Technology (IIT), in 2002 and 2009 respectively. He is the 2009 recipient of the Institute of Navigation (ION) Parkinson award, and the 2014 recipient of the ION's Early Achievement Award. He is currently a research assistant professor at IIT, working on multi-sensor integration, on sequential fault-detection for multi-constellation navigation systems, and on relative and differential receiver autonomous integrity monitoring (RAIM).

Yawei Zhai obtained a Bachelor degree in Mechanical Engineering from Qingdao University of Science and Technology, China, in 2013. He is currently a PhD candidate and Research Assistant in Mechanical and Aerospace Engineering at Illinois Institute of Technology (IIT). His research focuses on ground and airborne monitors for advanced receiver autonomous integrity monitoring (ARAIM) using multi-constellation global navigation satellite systems.

Dr. Boris Pervan is a Professor of Mechanical and Aerospace Engineering at IIT, where he conducts research on advanced navigation systems. Prior to joining the faculty at IIT, he was a spacecraft mission analyst at Hughes Aircraft Company (now Boeing) and a postdoctoral research associate at Stanford University. Prof. Pervan received his B.S. from the University of Notre Dame, M.S. from the California Institute of Technology, and Ph.D. from Stanford University. He is an Associate Fellow of the AIAA, a Fellow of the Institute of Navigation (ION), and Editor-in-Chief of the ION journal NAVIGATION. He was the recipient of the IIT Sigma Xi Excellence in University Research Award (2011, 2002), Ralph Barnett Mechanical and Aerospace Dept. Outstanding Teaching Award (2009, 2002), Mechanical and Aerospace Dept. Excellence in Research Award (2007), University Excellence in Teaching Award (2005), IEEE Aerospace and Electronic Systems Society M. Barry Carlton Award (1999), RTCA William E. Jackson Award (1996), Guggenheim Fellowship (Caltech

1987), and Albert J. Zahm Prize in Aeronautics (Notre Dame 1986).

ABSTRACT

This paper describes the design and preliminary evaluation of a new 'Online' ground monitor for advanced receiver autonomous integrity monitoring (ARAIM). ARAIM is intended for vertical guidance of aircraft down to 200 feet altitude. In ARAIM, fault detection is autonomously performed at the airborne receiver using dual-frequency, multi-constellation GNSS. The ARAIM ground monitor aims at validating the assertions made at the airborne receiver on 'integrity parameters', which include, for example, the ranging error variances and prior fault probabilities associated with satellite orbit and clock ephemeris errors. To determine these integrity parameters, two candidate architectures, Offline and Online, are under consideration. Both architectures assume the constellation service providers (CSP) satisfy their service performance commitments. But, in addition, Online ARAIM provides a set of precise 'overlay' orbit and clock ephemeris parameter predictions to replace the CSP navigation message. And, the Online monitor can broadcast hourly updates on the integrity parameters. It follows that probability bounds on integrity parameters can be tightened, which ultimately reduces availability risk as compared to the Offline architecture. On the other hand, Online ARAIM increases 'connectivity risk', as it requires monitor updates to be transmitted from the ground segment to the aircraft. This paper presents an Online monitor concept, which establishes a clear relationship between the monitor's detection test statistic, and the integrity parameters broadcast to the aircraft. The test statistic is derived independently from the Online overlay ephemeris, using code and carrier phase measurements collected at a few worldwide reference stations. Preliminary evaluation of the test statistic distribution is carried out using truth data from the International GNSS Service (IGS), and using covariance analysis. Results suggest that SV position and clock estimation, which is needed to establish the monitor test statistic, is achievable at the decimeter level using a sparse network of ground reference stations.

INTRODUCTION

This paper describes the design, analysis and evaluation of a new ground monitor for aircraft navigation using future dual-frequency, multi-constellation advanced receiver autonomous integrity monitoring (ARAIM). Unlike in Satellite-Based Augmentation Systems (SBAS), fault detection using ARAIM is autonomously performed at the airborne receiver. In ARAIM, the primary goal of the ground monitor is to validate, over hour-to-month-long periods, the assertions made at the airborne receiver.

Receiver autonomous integrity monitoring (RAIM) has been used for decades to mitigate the impact of rare-event faults including satellite clock and orbit ephemeris faults in global navigation satellite systems (GNSS) [1], [2]. For example, RAIM is used in aviation for horizontal positioning during en-route navigation. The core principle of RAIM is to exploit redundant GNSS ranging signals to achieve self-contained fault detection at the user receiver.

With the modernization of GPS, the full deployment of GLONASS, and the emergence of Galileo and Beidou, the number of redundant ranging signals increases dramatically, which opens the possibility to fulfill stringent navigation integrity requirements using RAIM. In particular, RAIM can help alleviate requirements on ground monitors. This is why researchers in the European Union and in the United States are investigating ARAIM, not only for horizontal en-route navigation, but also for worldwide vertical guidance of aircraft down to 200 feet altitude [3], [4], [5].

To incorporate information from multiple constellations at different stages of their development, ARAIM relies on an Integrity Support Message (ISM) generated at the ground and broadcast to airborne receivers. The ISM provides integrity parameters describing measurement errors and faults, including, for example, the prior probability of satellite fault, P_{sat} , and the standard deviation of nominal ranging measurement uncertainty due to satellite orbit and clock ephemeris errors, σ_{URA} [3], [4]. These integrity parameters are key inputs to the airborne ARAIM algorithm, which defines positioning error bounds called protection levels.

Candidate ARAIM architectures for ISM generation include ‘Offline’ and ‘Online’ architectures [4]. Both architectures assume the Constellation Service Providers (CSP) meet their Service Provider Commitments, thereby ensuring bounds on the ISM integrity parameter values. However, in contrast with Offline, the Online architecture gives the Air Navigation Service Provider (ANSP) more control over the ISM parameters by generating and broadcasting its own orbit and clock ephemeris parameters. This new ephemeris, named the ‘overlay’

ephemeris, is different from the one transmitted in the CSP navigation message.

As indicated in Fig. 1, the overlay is generated using a global network of sparsely-distributed, dedicated ground reference stations (RS). The overlay, primarily intended for aircraft users, is broadcast in the ISM in addition to the integrity parameters. For Online ARAIM, the ISM is broadcast hourly, versus monthly for Offline ARAIM. But, the Online approach can help mitigate the Offline ARAIM availability risk caused by potentially weak CSP commitments on the achievable ranging performance. In other words, if the CSP specifies large values for σ_{URA} and P_{sat} , the resulting service availability using Offline ARAIM is low. In contrast, Online ARAIM can tighten the bounds on these parameters by transmitting a precise orbit and clock ephemeris overlay.

A key component of Online ARAIM is the ground monitor. Its primary function is to ensure the consistency between the broadcast overlay performance and the ISM integrity parameters. Since ARAIM fault detection is performed at the airborne receiver, potential inconsistencies do not need to be communicated to the aircraft within a short time-to-alarm (as in SBAS). Instead, the ISM integrity parameters must take into account the hour-long ISM update interval. Also, in ARAIM, the ground monitor is running continuously, in the background of the actual integrity monitoring process at the aircraft. This Online ARAIM monitor does not require an integrity requirement allocation, which, again, is different from monitors used in SBAS.

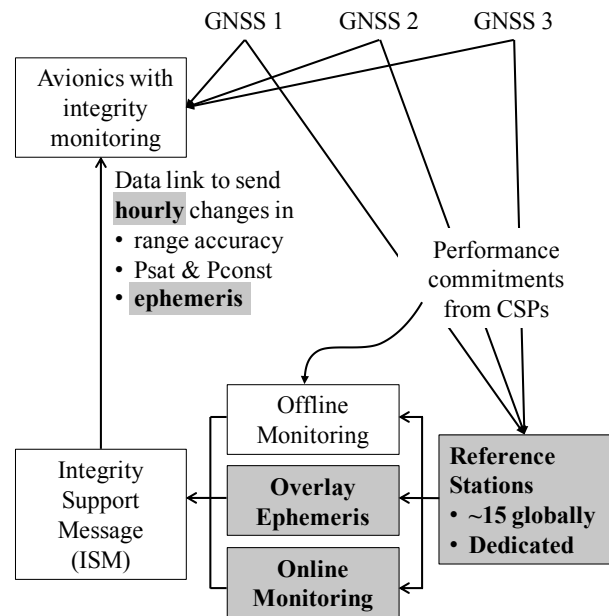


Fig. 1 Overview of the Online ARAIM Architecture (gray-shaded elements indicate differences with the Offline architecture) [4].

GROUND MONITOR CONCEPT

Motivation for a Simple ONM Monitor

In response, in this work, we develop a new Online Monitor (ONM) to ensure integrity of ephemeris overlay by establishing and controlling σ_{URA} , and P_{sat} . The ONM is designed to be much simpler than the overlay orbit determination process, thereby facilitating ISM generator certification to ensure safety critical hazardous operations.

In order to devise a cohesive integrity monitoring architecture, the paper first establishes the relationship between integrity parameters (σ_{URA} , and P_{sat}) and the ground monitor performance. The proposed monitor concept aims at detecting faults in the broadcast ephemeris. It is not intended to monitor against payload faults, even though it may provide a means to do so. In addition, the monitor exploits the fact that broadcast ephemerides have overlapping periods of validity. This is consistent with orbit and clock parameters transmitted in the GPS navigation message, which is typically updated every two hours but is valid over four hours [6]. Thus, the concept ONM can be used to monitor against faults in the overlay, as well as in the CSP ephemeris.

The paper then describes an example ONM implementation in three steps. First, the ONM determines the satellite positions independently of the overlay, using ground RS measurements and a simple parametric model (e.g., we use the GPS CNAV 23-parameter ephemeris model). Second, these ONM-generated satellite position estimates are subtracted from those obtained using the ephemeris overlay to produce a residual error history. Third, the residual error is processed using a straightforward ‘snapshot’ (instantaneous) monitor.

The first step in the process is crucial because the sensitivity of the monitor to ephemeris faults directly scales with the accuracy of the ONM-generated satellite position estimates. To investigate the feasibility of the ONM, a preliminary analysis is carried out. First, the impact on satellite positioning error of ground measurement uncertainty, including multipath and receiver noise, tropospheric delay, and errors in time-synchronization across RS, is evaluated using a covariance analysis. In parallel, the fidelity of the 23-parameter model is assessed. The model is fit to truth data obtained from precise, post-processed satellite clock and orbit data from the International GNSS Service (IGS). Residual errors from the covariance analysis and from the data fitting process amount to decimeter-level errors root-mean-squared. This preliminary analysis shows the potential of the ONM to distinguish nominal errors in the measured satellite positions from small-size, meter-level faults in the overlay.

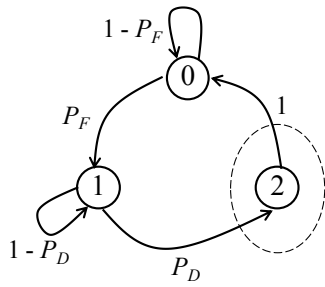
One of the main objectives of ARAIM is to fulfill an overall navigation integrity risk requirement noted I_{REQ} (e.g., $I_{REQ} = 10^{-7}$ [3]). The overlay ephemeris generation and dissemination process could be designed to ensure that the probability of occurrence of satellite ephemeris faults P_{sat} is negligibly small with respect to I_{REQ} . This would be a direct but costly approach, because all software and hardware components involved in this process would have to be certified to extremely stringent levels of integrity.

A more practical approach is to use a simple, certifiable ONM and an overlay with a reasonably small failure rate. For example, in GPS, the CSP Performance Standard [7] guarantees a satellite fault rate of $10^{-5}/\text{hr}$, and the GPS ground segment has historically detected faults within an hour [8], thereby establishing a prior probability of satellite fault P_{sat} of about 10^{-5} . Similarly, we want the ONM to be a simple process, derived and implemented independently of the overlay ephemeris. Integrity in ARAIM is then ensured at the airborne receiver.

Detection with Delayed Alert

A major challenge in the design of this monitor is that notifications to the aircraft only occur during ISM updates, e.g., at regular hour-long intervals. Let τ_{ISM} be the time interval between successive ISM updates.

In order to account for τ_{ISM} , we consider the Markov chain in Fig. 2. Assuming constant average failure and detection rates, the probability of fault and probability of detection are respectively noted P_F and P_D . The Markov chain in Fig. 2 includes a set of three mutually exclusive, exhaustive states (0, 1, and 2). The chain can be described starting at the fault-free state ‘0’. If a fault occurs with probability P_F , then the system transitions to state ‘1’, where a fault exists, but is undetected. From state ‘1’, if the fault is detected with probability P_D , then the chain does not directly go back to the fault-free state ‘0’. Instead, it leads to an intermediary state ‘2’, where a fault exists, is detected, but an alert can only be sent at the next ISM update. Only when the new ISM update is issued does the system get back to fault-free state ‘0’. Thus, the intermediary state ‘2’ captures the delay in alert, which can be as large as τ_{ISM} .



-
- 0: fault-free conditions
 - 1: fault exists, undetected
 - 2: fault exists, is detected, but alert can only be sent at next ISM update

Fig. 2 Markov Chain of Detection with Delayed Alert.

Assuming that the overlay ephemeris generation and Online monitoring are continuous processes, the steady-state performance of the system can be analyzed. Appendix A shows that the probability P_{sat} of a fault affecting the aircraft, i.e., the probability of being in states ‘1’ or ‘2’, as time approaches infinity, is given by:

$$P_{sat} = \frac{P_F + P_F P_D}{P_D + P_F + P_F P_D} \quad (1)$$

If the ONM detector is perfect, then $P_D = 1$. In addition, assuming an exponential distribution of faults (the exponential distribution is the only one assuming a constant average fault rate), then P_F can be expressed as:

$$P_F = \frac{\tau_{ISM}}{MTBF} \quad (2)$$

where $MTBF$ is the mean time between failures of the overlay ephemeris, and where τ_{ISM} is much smaller than $MTBF$. In this case, P_{sat} becomes:

$$P_{sat} = \frac{2\tau_{ISM}}{MTBF + 2\tau_{ISM}} \quad (3)$$

Equation (3) is analyzed in Fig. 3 for varying values of the desired P_{sat} versus required $MTBF$ of the overlay generation process. Results are presented for color-coded values of τ_{ISM} ranging from five minutes (blue curve) to four hours (red). Fig. 3 shows that for the τ_{ISM} -value of one hour (green curve), if the desired P_{sat} is 10^{-5} ($P_{sat} = 10^{-5}$ is assumed in ARAIM sensitivity analyses in [4]), then the required $MTBF$ is 22 years. For comparison, the specified $MTBF$ for GPS, which is the

most reliable and mature GNSS, is about 10 years per satellite. This number is derived from the commitment by GPS to have no more than three major service failures per year for the entire GPS constellation [7]. Thus, the 22 year $MTBF$ for the overlay ephemeris would be extremely challenging to fulfill (and this number assumes a perfect detector, $P_D = 1$).

Fig. 3 also shows that the $MTBF$ requirement can be relaxed by considering more frequent ISM updates. For example, for a τ_{ISM} of 15 minutes (second blue curve), the $MTBF$ required to achieve $P_{sat} = 10^{-5}$ is only 8 years. But, a 15 minute τ_{ISM} puts additional constraints on the connectivity between ground and aircraft.

Detection with Advanced Alert

As an alternative to relax the overlay ephemeris $MTBF$ requirement, an advanced alert detection concept is proposed, based on the following three assumptions.

- The ONM aims at detecting against orbit and clock ephemeris faults, not against satellite payload faults.
- Overlay ephemerides are updated every hour, and are valid over overlapping one-hour intervals, as displayed in Fig. 4.
- For a given ephemeris, a fault is equally observable throughout its period of validity; i.e., the error profile over the first hour is representative of the behavior during the second hour.

The second assumption on overlapping ephemerides is consistent with GPS ephemerides, typically updated every two hours, but valid over 4 hours; GPS ephemerides can therefore also be monitored using the ONM.

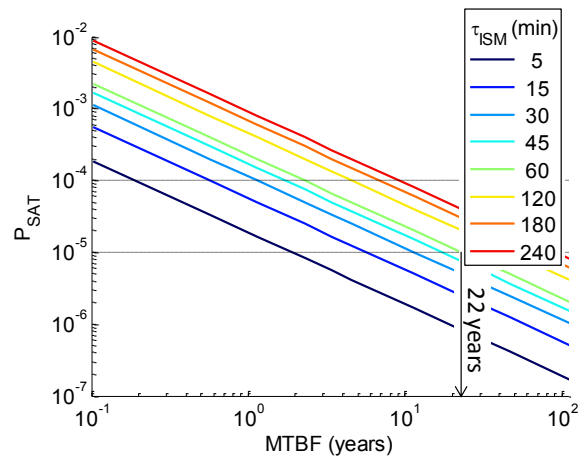


Fig. 3 Desired Probability of Satellite Fault at Aircraft (P_{sat}) Versus Required $MTBF$ for the Ground’s Overlay Ephemeris, for Varying Values of the ISM Update Interval (Assuming ‘Perfect’ Detector with Delayed Alert).

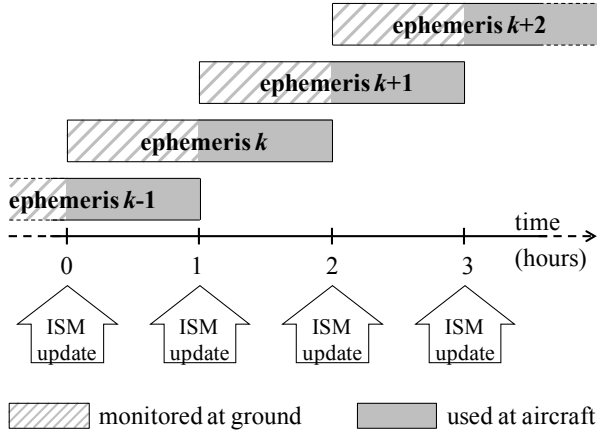
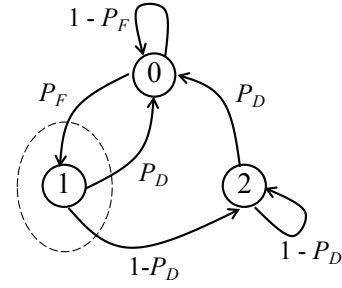


Fig. 4 Online Monitor Concept Under the Overlapping Ephemeris Assumption.

As illustrated in Fig. 4, two valid broadcast overlay ephemerides are continuously available to the user. In this concept monitor, the aircraft uses the oldest ephemeris, while the most recent is being monitored by the ground. For example, between hours 0 and 1, the aircraft uses ephemeris $k-1$, and the ONM monitors ephemeris k . Between hours 1 and 2, if ephemeris k was validated by the ONM, then the aircraft uses it without having been exposed to an unmonitored ephemeris between ISM updates.

It can be noted that there are special cases where the aircraft may not have access to the oldest of the two overlapping ephemerides, e.g., if the airborne receiver has been operating for less than an hour at the start of the approach. In this case, several alternative solutions can be considered: the old ephemeris could be loaded at take-off; or, both ephemerides could be transmitted in the ISM; or, the aircraft could use CSP ephemerides monitored by the Offline ARAIM function if the corresponding integrity parameters are broadcast (they represent a much smaller amount of data than the overlay ephemeris).

The advanced alert detection process is modeled using the Markov chain presented in Fig. 5. Similar to Fig. 2, the Markov chain includes three states, and is described starting from the fault-free state '0'. If a fault occurs, the system transitions into a *latent fault* state '1', where the fault on the most recent ephemeris can be seen at the ground, but is not at the aircraft yet. If the fault is detected at state '1', then the system goes back to fault-free conditions without ever affecting the aircraft. Conversely, if the fault is not detected at state '1', then the system enters the *active fault* state '2', where the fault impacts the aircraft. In state '2', the fault is still observable at the ground, which has further opportunities to detect (with probability P_D) and alert (at the next ISM update), thereby bringing the system back to fault-free conditions.



- 0: fault-free conditions
- 1: latent fault exists at ground, but not at aircraft yet
- 2: active fault exists, not only at ground but also at aircraft

Fig. 5 Markov Chain of Detection with Advanced Alert.

In this case, P_{sat} is the probability of being in state '2' as time approaches infinity, which Appendix B proves is given by:

$$P_{sat} = \frac{P_F - P_F P_D}{P_F + P_D} \quad (4)$$

In contrast with equation (1), equation (4) shows that a perfect detector ($P_D = 1$) can reduce P_{sat} to zero. More realistically, the probability of detection P_D will vary with fault magnitude f . As f increases, P_D approaches one. This dependency on f is captured in the following equation:

$$P_{sat}(f) = \frac{P_F - P_F P_D(f)}{P_F + P_D(f)} \quad (5)$$

where P_F is a function of the *MTBF* specified by overlay generation system. Further evaluation of P_F is outside the scope of this paper. This paper focuses on $P_D(f)$, which is defined by the ONM.

Let q be the ONM detection test statistic. $P_D(f)$ can be expressed in terms q as:

$$P_D(f) = P(q \geq T | f) \quad (6)$$

where T is the detection threshold set to limit loss of availability under fault-free conditions. We assume that the aircraft does not use updated ISM information received during the short (150 sec) duration of an

approach; therefore broadcast ONM notifications do not cause mission interruptions (i.e., loss of continuity). Thus, T is not set to satisfy a continuity requirement (as is often the case, e.g., in [9], [10], [11]), but instead to meet an availability requirement.

In parallel, we define the statistic q in equation (6) as part of the ONM design. If the probability distribution of q is known, then $P_D(f)$ can be evaluated for any f . In particular, the fault magnitude f_* can be determined, which provides a $P_D(f_*)$ such that the resulting $P_{sat}(f_*)$ is acceptable – for example, $P_{sat} = 10^{-5}$ as assumed in [4].

Finally, let σ_{URA} be the standard deviation of the ranging measurement uncertainty due to satellite orbit and clock errors (also referred to as user range accuracy or URA). Reference [7] defines a fault f_* as an error exceeding a multiple of σ_{URA} , i.e., as:

$$f^* \geq Q^{-1}(P_{sat}/2)\sigma_{URA} \quad (7)$$

where $Q^{-1}(\cdot)$ is the inverse tail probability function of the standard normal distribution. f_* is defined in [7] as $4.42\sigma_{URA}$ for $P_{sat} = 10^{-5}$. (Reference [7] also suggests that nominal ephemeris errors ε are over-bounded in the cumulative distribution function (CDF)-sense [12] by a zero-mean normal distribution with standard deviation σ_{URA} for $\varepsilon < f_*$. The validity of the Gaussian over-bound can be ensured using Offline monitoring methods described in [4].)

Equations (5) to (7) establish an analytical relationship between the *MTBF* specified by the ground's overlay ephemeris generation system, the detection performance of the ground's ONM, the desired P_{sat} at the aircraft, and the achievable σ_{URA} at the aircraft. This relationship is crucial for the design, analysis, and implementation of the ONM. First, equations (5) to (7) provide the means to determine the achievable σ_{URA} -value using the Online ARAIM architecture. (Reducing σ_{URA} is the primary motivation for the Online architecture as it is shown in [4] to have a dramatic impact on availability performance.) Second, equations (5) to (7) will be used operationally to validate P_{sat} and σ_{URA} values broadcast to the aircraft, based on the ground's overlay generation and ONM detection performance.

The next sections define a preliminary version of the ONM detection test statistic q in equation (6), and evaluate the main sources of error impacting q .

GROUND MONITOR DESIGN

This section describes an example ONM implementation in three steps. First, the ONM determines the position and clock deviations for each satellite individually. Second, these ONM-generated satellite position estimates are subtracted from those independently obtained using the ephemeris overlay. Third, the residual error profile is analyzed to define the ONM detection test statistic.

Step 1: Truth Orbit Determination

The ONM uses measurements from a global, sparse network of dedicated ground reference stations (RS). In this paper, we consider an example network of 17 RS collocated with GPS monitor stations (shown in Fig. 6).

This network ensures that each satellite can continuously be tracked by at least two reference stations, which provides redundancy in case of single-RS failure. This sparse network does not allow reverse positioning (four RS simultaneously observing a space vehicle (SV) are required to directly estimate the satellite position – this network only guarantees continuous tracking by two stations). Instead, the ONM determines SV trajectories using measurements collected over time, and using a dynamic model of the satellite orbit and clock. To facilitate certification, we use a simple parametric model.

For example, in this paper, we use the GPS CNAV 23-parameter orbit and clock ephemeris model [6]. Let \mathbf{p}_i be the 23×1 vector of GPS ephemeris model parameters for satellite i , and let $\mathbf{g}(\mathbf{p}_i)_k$ be the 4×1 vector of satellite position and clock offset (with respect to GPS time) derived from the model at time k . The true position $\mathbf{x}_{i,k}$ and clock offset $\tau_{i,k}$ of satellite i at time k can be expressed as:

$$\begin{bmatrix} \mathbf{x}_{i,k} \\ \tau_{i,k} \end{bmatrix} = \mathbf{g}(\mathbf{p}_i) + \begin{bmatrix} \Delta\mathbf{x}_{i,k} \\ \Delta\tau_{i,k} \end{bmatrix} \quad (8)$$

where $\Delta\mathbf{x}_{i,k}$ and $\Delta\tau_{i,k}$ are the deviations between $\mathbf{x}_{i,k}$ and $\tau_{i,k}$ and the position and clock derived from the orbit model $\mathbf{g}(\mathbf{p}_i)_k$. $\Delta\mathbf{x}_{i,k}$ and $\Delta\tau_{i,k}$ represent the model's inability to perfectly capture the true orbit.

The GPS orbit model is valid over a four-to-six-hour time interval noted T_{FIT} [6]. (Sensitivity to T_{FIT} is evaluated in the next section.) The following paragraphs describe the ONM's method to determine the ephemeris parameters \mathbf{p}_i , for which the model best fits the measurements collected at the RS over T_{FIT} .

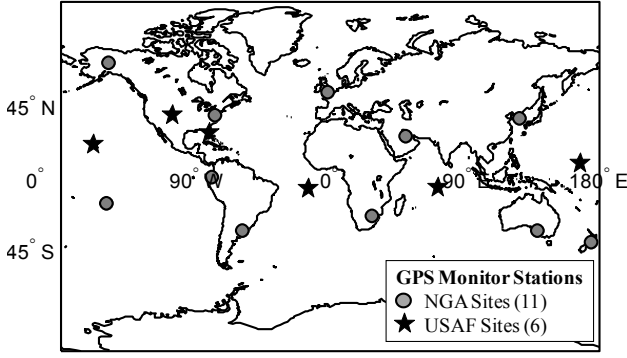


Fig. 6 Example Network of Ground Reference Stations Used in the Online Monitor Evaluation.

Dual-frequency code and carrier measurements from satellite i , received at RS j , at time k , are respectively expressed as:

$${}^{i,j}\rho_k = \|\mathbf{x}_j - \mathbf{x}_{i,k}\| + \tau_{i,k} + {}^{i,j}\varepsilon_{\rho,k} \quad (9)$$

$${}^{i,j}\phi_k = \|\mathbf{x}_j - \mathbf{x}_{i,k}\| + \tau_{i,k} + {}^{i,j}\eta + {}^{i,j}\varepsilon_{\phi,k} \quad (10)$$

where

- \mathbf{x}_j is the known location of RS j , for example, in and Earth-Centered Earth-Fixed (ECEF) reference frame
- $\mathbf{x}_{i,k}$ is the unknown location of SV i at time k
- $\tau_{i,k}$ is the unknown clock offset of SV i at time k
- ${}^{i,j}\eta$ is the unknown, constant carrier phase cycle ambiguity for SV i at RS j
- $\|\ \|\$ is the Euclidean norm operator, in this case providing the distance between RS j and SV i .

The code and carrier phase measurement error terms are respectively noted ${}^{i,j}\varepsilon_{\rho,k}$ and ${}^{i,j}\varepsilon_{\phi,k}$. They account for receiver noise, multipath error, tropospheric delay, and errors in the time-transfer process required to synchronize reference stations. A detailed measurement error model, accounting for time-correlation and for correlation across RS is given in Appendix C.

A Newton-Raphson process (e.g., described in [13]) is employed to iteratively estimate the ephemeris parameters \mathbf{p}_i . We can use the CSP ephemeris parameters as an initial guess $\bar{\mathbf{p}}_i$ for \mathbf{p}_i . First, equation (10) is linearized about an initial guess $\mathbf{g}(\bar{\mathbf{p}}_i)_k$ of $\mathbf{x}_{i,k}$ and $\tau_{i,k}$. Then, equation (8) is linearized about $\bar{\mathbf{p}}_i$. (This two-step process could equivalently be performed in a single step,

but the intermediary result will become useful later in the paper). Substituting the result of the second linearization step into the first one yields the following equation:

$${}^{i,j}\delta\rho_k = \begin{bmatrix} {}^{i,j}\mathbf{e}_k^T & 1 \end{bmatrix} \mathbf{A}_{i,k} \delta\mathbf{p}_i + {}^{i,j}\varepsilon_{\rho,k} \quad (11)$$

where

δ 's indicate deviations from nominal values. Nominal values are iteratively refined as part of the Newton-Raphson process.

${}^{i,j}\mathbf{e}_k$ is the 3×1 unit line of sight vector between SV i and RS j at time k in ECEF

$\mathbf{A}_{i,k}$ is a 4×23 matrix of numerically-derived partial derivatives of the position coordinates of SV i at time k over the ephemeris parameters:

$$\mathbf{A}_{i,k} = \begin{bmatrix} \partial x_{i,k} / \partial p_1 & \partial y_{i,k} / \partial p_1 & \partial z_{i,k} / \partial p_1 & \partial \delta \tau_{i,k} / \partial p_1 \\ \vdots & \vdots & \vdots & \vdots \\ \partial x_{i,k} / \partial p_{23} & \partial y_{i,k} / \partial p_{23} & \partial z_{i,k} / \partial p_{23} & \partial \delta \tau_{i,k} / \partial p_{23} \end{bmatrix}^T$$

We used the notations: $\delta\mathbf{x}_{i,k} = [x_{i,k} \ y_{i,k} \ z_{i,k}]^T$ and $\delta\mathbf{p}_i = [p_1 \ \dots \ p_{23}]^T$.

The parameters to be estimated or 'states' are $\delta\mathbf{p}_i$. To do so, measurements ${}^{i,j}\delta\rho_k$ and state coefficients $[\begin{smallmatrix} {}^{i,j}\mathbf{e}_k^T \\ 1 \end{smallmatrix}] \mathbf{A}_{i,k}$ are stacked over T_{FIT} , from time 1 to time K . The resulting measurement vector and state coefficient matrix are written as:

$${}^{i,j}\delta\mathbf{p} = \begin{bmatrix} {}^{i,j}\delta\rho_1 \\ \vdots \\ {}^{i,j}\delta\rho_K \end{bmatrix} \quad \text{and} \quad {}^{i,j}\mathbf{B} = \begin{bmatrix} [\begin{smallmatrix} {}^{i,j}\mathbf{e}_k^T \\ 1 \end{smallmatrix}] \mathbf{A}_{i,1} \\ \vdots \\ [\begin{smallmatrix} {}^{i,j}\mathbf{e}_k^T \\ 1 \end{smallmatrix}] \mathbf{A}_{i,K} \end{bmatrix} \quad (12)$$

Measurements and state coefficients are then stacked for all RS tracking SV i during T_{FIT} , i.e., for RS 1 to J . The resulting code measurement vector and state coefficient matrix are given by:

$${}^i\delta\mathbf{p} = \begin{bmatrix} {}^{i,1}\delta\mathbf{p} \\ \vdots \\ {}^{i,J}\delta\mathbf{p} \end{bmatrix} \quad \text{and} \quad {}^i\mathbf{B}_\rho = \begin{bmatrix} {}^{i,1}\mathbf{B} & \mathbf{0}_{K \times 1} & & \mathbf{0}_{K \times 1} \\ \vdots & & \ddots & \\ {}^{i,J}\mathbf{B} & \mathbf{0}_{K \times 1} & & \mathbf{0}_{K \times 1} \end{bmatrix} \quad (13)$$

where $\mathbf{0}_{a \times b}$ is an $a \times b$ matrix of zeros. To lighten notations, we assumed that all RS track SV i over K time epochs.

The same operation is carried out for carrier measurements, for which state coefficients include one's for constant cycle ambiguities that must be estimated as well. The resulting state coefficient matrix is:

$${}^i\mathbf{B}_\phi = \begin{bmatrix} {}^{i,1}\mathbf{B} & \mathbf{1}_{K \times 1} & & \mathbf{0}_{K \times 1} \\ \vdots & & \ddots & \\ {}^{i,J}\mathbf{B} & \mathbf{0}_{K \times 1} & & \mathbf{1}_{K \times 1} \end{bmatrix} \quad (14)$$

where $\mathbf{1}_{a \times b}$ is an $a \times b$ matrix of one's.

Finally, code and carrier measurements, and their corresponding state coefficients, are stacked together as follows:

$$\mathbf{z}_i = \begin{bmatrix} {}^i\delta\mathbf{p}^T & {}^i\delta\boldsymbol{\phi}^T \end{bmatrix}^T \quad \text{and} \quad \mathbf{B}_i = \begin{bmatrix} {}^i\mathbf{B}_\rho^T & {}^i\mathbf{B}_\phi^T \end{bmatrix}^T \quad (15)$$

The weighted least-squares estimate of the orbit parameter vector for SV i , over T_{FIT} , is obtained using the following equation:

$$\delta\mathbf{p}_i = \left(\mathbf{B}_i^T \mathbf{V}_i^{-1} \mathbf{B}_i \right)^{-1} \mathbf{B}_i^T \mathbf{V}_i^{-1} \mathbf{z}_i \quad (16)$$

where \mathbf{V}_i is the measurement error covariance matrix discussed in Appendix C. Equation (16) is used in the Newton-Raphson process to fit the 23-parameter model to the RS measurements. The resulting orbit and clock estimates are determined using a simple, certifiable process, independently of the overlay ephemeris.

Step 2: 'Overlay Minus ONM' Residual Error

As shown in Fig. 4, at each ISM update, the ONM evaluates the new overlay ephemeris over one hour. The estimated satellite orbit and clock derived from the overlay are then compared to the ONM-generated estimates over the same period.

The orbit and clock estimates obtained from the overlay ephemeris should be as precise, or probably even more precise than the ones derived by the ONM. On the one hand, overlay ephemeris are *predicted*, not directly estimated using *current time* measurements as in the ONM. But, on the other hand, the overlay's orbit and clock determination process can be much more elaborate than simply fitting a 23-parameter model to data.

The difference between the overlay and the ONM satellite position and clock estimates, $\mathbf{x}_{LAY,i,k}$, and that of the ONM, $\mathbf{x}_{ONM,i,k}$, at time k , is expressed as:

$$\mathbf{r}_{i,k} = \mathbf{x}_{ONM,i,k} - \mathbf{x}_{OVL,i,k} \quad (17)$$

Let us finally express the residual errors in a satellite-fixed local-level (LL) {radial, in-track, cross-track} reference frame as:

$$\mathbf{r}_{LL,i,k} = \mathbf{R}_{LL,i,k} \mathbf{r}_{i,k} \quad (18)$$

where

- $\mathbf{r}_{LL,i,k}$ is the LL 'overlay minus ONM' residual
- $\mathbf{r}_{i,k}$ is the ECEF residual
- $\mathbf{R}_{LL,i,k}$ is the ECEF to LL rotation matrix

Step 3: Monitor Test Statistic Definition

The output of Step 2 is a 4×1 residual vector $\mathbf{r}_{LL,i,k}$ in equation (17). A straightforward detection test could be carried out based on the weighted norm $\mathbf{r}_{i,k}$. This would mean that SV positioning uncertainties are equally treated in all three LL position coordinates. However, it is known that, for aircraft users near the surface of the earth, SV radial positioning and clock errors have a larger impact than non-radial positioning errors. As illustrated in Fig. 7, the worst-case impact for any user on earth of non-radial positioning errors is obtained using a scaling factor of approximately 0.24.

In this paper, to account for this geometric constraint, we evaluate the signal in space range error (SISRE) [14], [15], [16]. Multiple versions of SISRE can be found in the literature. We consider the following equation:

$$r_{SISRE,i,k} = (r_{R,i,k} + r_{CLK,i,k}) + 0.24 \operatorname{sgn}(r_{R,i,k} + r_{CLK,i,k}) \sqrt{r_{A,i,q}^2 + r_{C,i,q}^2} \quad (19)$$

where

- $r_{R,i,k}$ the radial position component of the residual
- $r_{A,i,k}$ the along-track position component
- $r_{C,i,k}$ the cross-track position component
- $r_{CLK,i,k}$ the clock component (in unit length)

Let n_{MON} be the number of sample residuals collected over the one hour monitoring period. For each SV i , a residual profile $r_{SISRE,i,k}$, for $k = 1, \dots, n_{MON}$, is obtained. This error profile is used to establish a detection test statistic. For example, a straightforward 'snapshot' monitor can be considered, where the statistic q_i for SV i is the largest residual over the monitoring period:

$$q_i = \max_{k=1, \dots, n_{MON}} \{r_{SISRE,i,k}\} \quad (20)$$

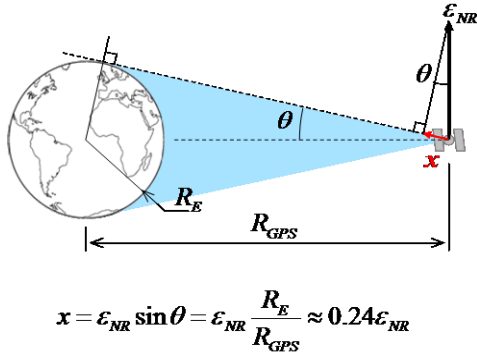


Fig. 7 Worst-Case Projection of Non-Radial SV Positioning Error.

This test statistic q_i can be used in equations (5) to (7) to determine the σ_{URA} -value achievable using Online ARAIM. At present, there is not enough publicly available information to evaluate the overlay ephemeris performance. The next section therefore focuses on error sources impacting Step 1. These error sources will probably be the largest contributors to the uncertainty in q_i .

PRELIMINARY GROUND MONITOR EVALUATION

This section aims at assessing the ONM performance in Step 1 of its derivation, i.e., at answering the following question: how well can satellite positions and clock be estimated using a sparse network of reference stations?

A two-step evaluation of the ONM-generated orbit and clock estimates is presented. First, a covariance analysis is used to evaluate the impact of RS measurement errors on the estimated SV position, assuming that the 23-parameter orbit model perfectly fits the true orbits. Then, assuming perfect measurements, we quantify the fidelity of the 23-parameter model to true GPS orbit data obtained from the International GNSS Service (IGS), for all satellites over multiple days.

Covariance Analysis

With the notations of equations (8) to (19), the position and clock estimate error covariance in a LL reference frame, for SV i at time k , using measurements collected over T_{FIT} at all RS, is expressed as:

$$\mathbf{P}_{LL,i,k} = \mathbf{R}_{LL,i,k} \mathbf{A}_{i,k} \left(\mathbf{B}_i^T \mathbf{V}_i^{-1} \mathbf{B}_i \right)^{-1} \mathbf{A}_{i,k}^T \mathbf{R}_{LL,i,k}^T \quad (21)$$

The diagonal elements of $\mathbf{P}_{LL,i,k}$ are the variances of the clock and orbit errors in LL reference frame. This

covariance analysis focuses on the radial positioning error component because it is the largest contributor to SISRE [14], [15], [16]. (The distribution of the non-linear SISRE equation (19) makes it difficult to determine its distribution. This issue will be addressed in future work.)

To illustrate the orbit estimation process, a single four-hour long SV trajectory is first represented in Fig. 8. The satellite ground track is displayed with multiple overlapping lines, which are color-coded consistently with RS: colors indicate at which point the SV is tracked by which RS.

Figure 9 shows the radial satellite positioning deviation profile over the four hour T_{FIT} . The standard deviation varies between 0.09m and 0.14 m. The lower chart in Fig. 9 shows that the satellite was continuously tracked by at least four and up to six RS.

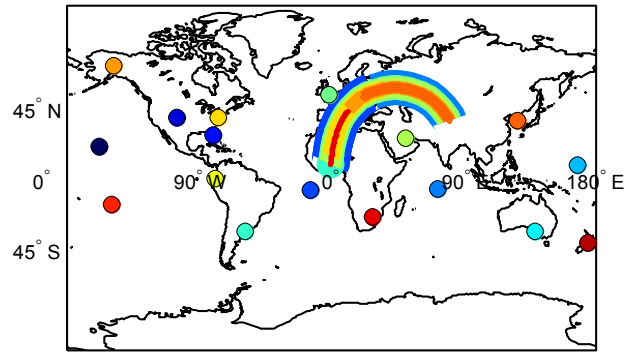


Fig. 8 Example Four-Hour-Long Satellite Pass Tracked By Six out of 17 Ground Reference Stations (the color code identifies different RS).

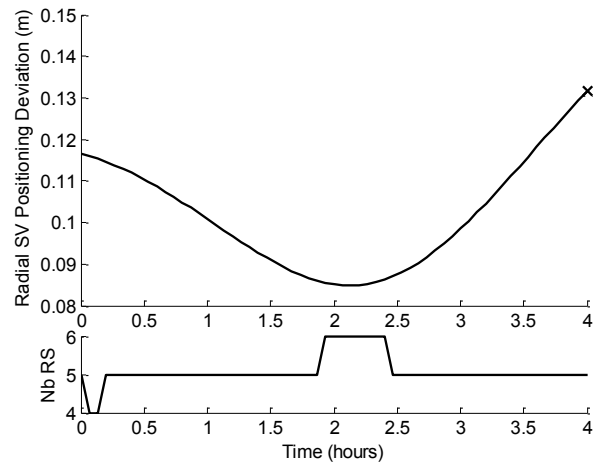


Fig. 9 Time-Profile of the Radial SV Positioning Error Standard Deviation (top) and Number of RS Tracking the SV (bottom) for a Four-Hour Fit Interval

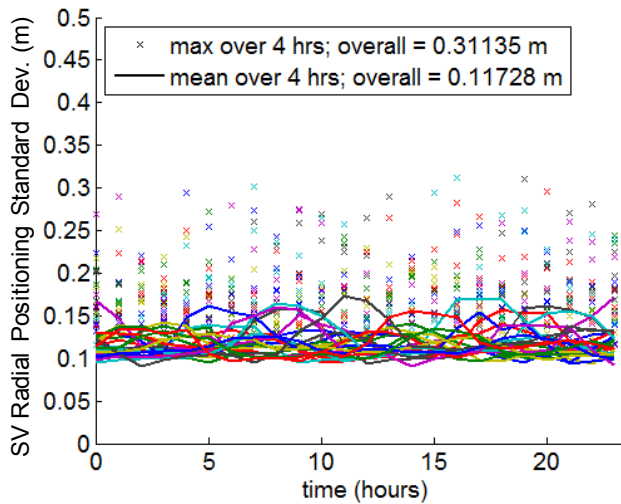


Fig. 10 Maximum and Mean Radial SV Positioning Error Standard Deviations for Time-Profiles Starting At Regular One-Hour Intervals Over 24 Hours, for All Satellites (the color code identifies different SVs).

This process is repeated in Fig. 10 for all satellites of a nominal 24-SV GPS constellation [6], for four-hour long fitting periods starting at regular 30 minute intervals. In Fig. 10, satellite PRNs are color-coded. Crosses represent maximum values of the standard deviations within each T_{FIT} -profile. For example, in Fig. 9, the max value is identified by a cross (rightmost point of the curve); such a value is represented in Fig. 10 at each half hour, and for each satellite. Overall, these max values do not exceed 0.31 m (as indicated in the figure legend). In addition, solid lines show mean values of the radial SV positioning error standard deviations within each fit interval. Mean values vary from about 0.08 m to 0.17 m, with an overall mean of 0.12 m.

The results in Fig. 10 indicate that high accuracy (decimeter level) ONM estimation of the orbit parameters is possible. But, they do not quantify modeling errors using the GPS CNAV 23-parameter ephemeris model.

Fidelity of GPS Ephemeris Orbit and Clock Model to Data

The above covariance analysis quantifies SV positioning errors assuming that the parametric model perfectly captures the true orbit and clock. But, because the model uses a small, finite number of parameters, residual model errors remain, which are evaluated in this section.

Precise orbit and clock ‘truth’ data is obtained from IGS, which is accurate to within five centimeters [17]. To evaluate model error, the GPS CNAV 23-parameter model [7] is fit to IGS truth data over 4 hour intervals. This operation is repeated over a 10-day period from

01/01/2014 to 01/10/2014, for all healthy GPS satellites. Figure 11 shows typical time-profiles of radial position error (thin solid lines) and SISRE (thick lines) for PRN5, over a 24 hours (on 01/01/2014). The color-code helps distinguish different four-hour-long fit intervals. Vertical t_{oe} -lines indicates the time of ephemeris, which is at the centre of each overlapping four-hour window. The results show that orbit model accuracy relative to truth appears to be about 0.05 m root-mean-squared (RMS) over four hours.

Figure 12 uses the same approach as in Fig. 11 to quantify residual model errors, which are root-mean-squared for all time-profiles over 10 days (for $T_{FIT} = 4$ hours), and for each satellite. In this case, the color code indicates different SV block types. Overall residual model error (RMS SISRE) per block type are given in legend: they range from 0.16 m for block II-A SVs to 0.06 m for block II-R-M SVs. Overall maximum errors range from 0.78 m for block II-A SVs to 0.34 m for block II-R-M SVs.

It is worth noting that the most recent block II-F satellites do not seem to perform better than the earlier block II-R and II-R-M satellites. This is caused by outlier results for PRN1 and PRN24. In both cases, we have determined that these larger RMS and maximum SISRE values are caused by clock errors. Clock errors for PRN1 and PRN24 are respectively plotted in Fig. 13 and 14. (These error profiles are obtained by fitting the ephemeris clock model (quadratic fit) to IGS clock data.) PRN24 is the only satellite using a Cesium clock, which is less accurate than Rubidium clocks used on other SVs [18]. PRN24 is therefore expected to exhibit larger clock errors. The periodic noisy error profile shown in Fig. 13 (and repeated over the ten day evaluation period) could be explained by the fact that PRN1 probably was in eclipse season [18]. This is supported by the fact that PRN1’s erratic clock behavior is no longer observed in July 2014.

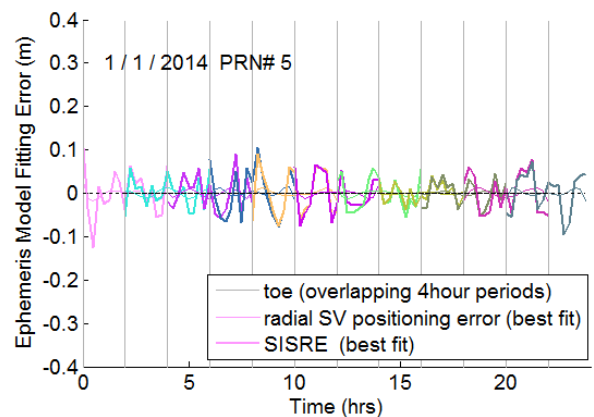


Fig. 11 Residual Error Profiles (‘Model minus Truth’) for Four-Hour Fitting Periods Starting at Regular Two-Hour Intervals Over 24 Hours, for PRN5 (the color code identifies different fit intervals).

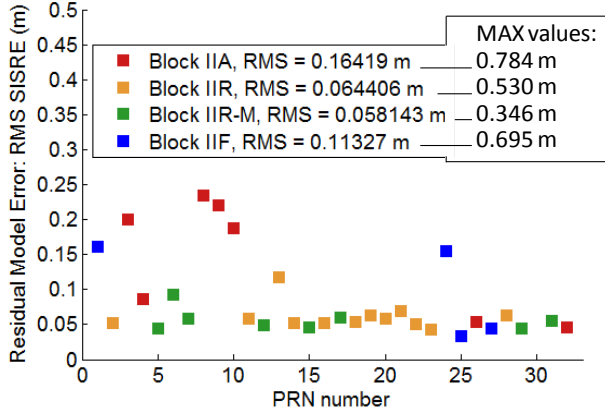


Fig. 12 RMS Residual Errors (‘Model minus Truth’) for Four-Hour Fitting Periods Over 10 Days, for All Satellites (the color code identifies SV block types).

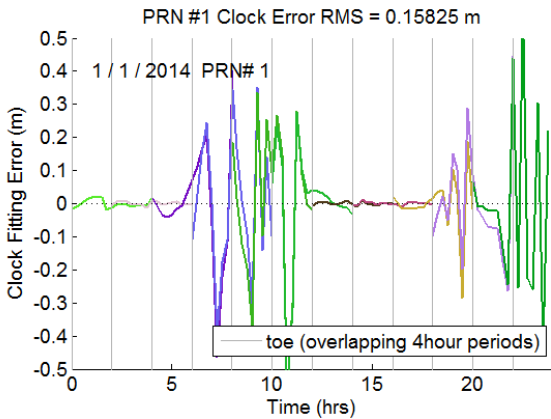


Fig. 13 Residual Clock Error Profiles for PRN1 (the color code identifies different fit intervals).

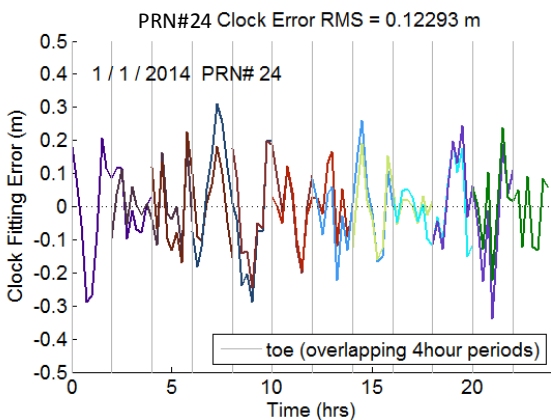


Fig. 14 Residual Clock Error Profiles for PRN24 (the color code identifies different fit intervals).

Sensitivity of Estimation Errors to Parametric Orbit and Clock Model

The GPS CNAV 23-parameter orbit and clock model was selected for its relative simplicity. To illustrate the impact of the parametric model, Fig. 15 shows residual model errors obtained using the legacy GPS 18-parameter orbit and clock model (currently broadcast by most GPS SVs). The RMS SISRE results are represented with white-filled squares for the legacy model, and with color-filled squares for the CNAV model. Overall RMS results per block-type are given in legend for the legacy model. As expected, model errors are significantly reduced using the 23-parameter model as compared to the 18-parameter model.

Sensitivity of Orbit and Clock Estimation to Fit Interval

To provide insight into the fitting process, Fig. 16 shows the maximum radial positioning standard deviations (from covariance analysis) and the RMS SISRE of the residual model error (‘model minus truth’) for varying values of the fit interval T_{FIT} . On the one hand, the longer T_{FIT} is, the lower the positioning standard deviation becomes, because measurement errors are averaged over longer periods. On the other hand, residual model errors increase with T_{FIT} because the true orbit profile becomes more complex while the parametric model remains unchanged (based on the same 23 parameters). Figure 16 suggests that the choice of $T_{FIT} = 4$ hours was pertinent.

Summary for the Preliminary Performance Evaluation

This section has identified and evaluated two primary sources of error affecting the ONM detection test statistic. First, the radial SV positioning error standard deviation caused by RS measurement errors was evaluated to range between the following values:

$$0.1 \text{ m} \leq \sigma \leq 0.3 \text{ m} \quad (22)$$

Then, the RMS SISRE caused by model errors is expected to be within the following bounds:

$$0.05 \text{ m} \leq b \leq 0.7 \text{ m} \quad (23)$$

The upper value in that range really is conservative because multi-constellation ARAIM in the next decade will probably only use the most recent SVs (block II-A satellites will no longer be operational), and because the outlier clock errors observed on PRN1 and PRN24 can reliably be predicted, and therefore mitigated.

These results are promising because if the lower bounds in equations (22) and (23)

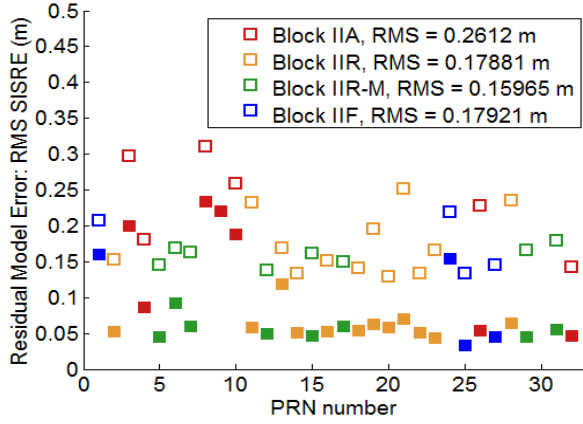


Fig. 15 Model Error Comparison Between the CNAV 23-Parameter Model and the Legacy 18-Parameter Model (the color code identifies SV block types).

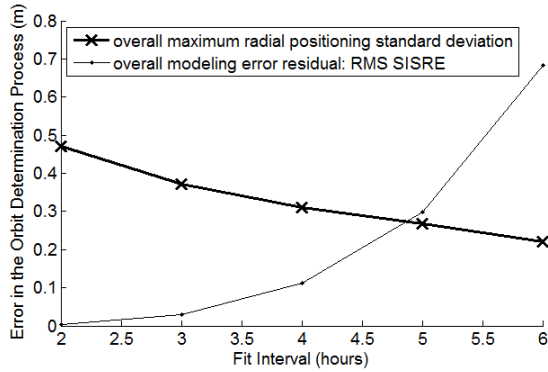


Fig. 16 Impact of the Fit Interval on Radial Positioning Standard Deviations and on RMS Residual Errors ('Model minus Truth').

CONCLUSION

This paper describes the design and preliminary evaluation of a new ONline Monitor (ONM) for dual-frequency, multi-constellation ARAIM. Ground monitoring methods are established to validate the integrity parameters that are then used at the airborne ARAIM algorithm to guarantee navigation safety.

The ONM exploits hourly updates of the integrity support message (ISM) to detect overlay ephemeris faults and send alerts. The paper makes relevant assumptions under which the ONM detection capability at the ground is directly linked to integrity parameters broadcast to the aircraft in the ISM. These parameters include the ranging error variance and the prior fault probability associated with satellite orbit and clock ephemeris errors. The paper introduces a new Online ARAIM detection method with advanced alert, which provides the means to tighten the

bounds on the integrity parameters as compared to Offline ARAIM.

A preliminary evaluation of the ONM is carried out to quantify the improvement brought by Online ARAIM. Ground station measurement uncertainty and SV clock and orbit model errors are identified as two primary sources of error affecting the ONM detection test statistic. Results suggest that decimeter-level satellite position and clock estimation errors can be achieved, but further analysis is required to determine the distribution of the ONM detection test statistic.

APPENDIX A: SATELLITE FAULT PROBABILITY USING DETECTION WITH DELAYED ALERT

This appendix provides a derivation for equation (1). The Markov chain in Fig. 2 can be expressed in equation form as:

$$P_0(k+1) = (1 - P_F)P_0(k) + P_2(k) \quad (\text{A.1})$$

$$P_1(k+1) = P_F P_0(k) + (1 - P_D)P_1(k) \quad (\text{A.2})$$

$$P_2(k+1) = P_D P_1(k) \quad (\text{A.3})$$

At steady state, equations (A.1) to (A.3) become:

$$P_0 = (1 - P_F)P_0 + P_2 \quad (\text{A.4})$$

$$P_1 = P_F P_0 + (1 - P_D)P_1 \quad (\text{A.5})$$

$$P_2 = P_D P_1 \quad (\text{A.6})$$

Equations (A.4) and (A.5) can be rewritten as:

$$P_2 = P_F P_0 \quad (\text{A.7})$$

$$P_1 = \frac{P_F}{P_D} P_0 \quad (\text{A.8})$$

In addition, since state '0' to '2' compose a set of mutually exclusive, exhaustive events, the following equation is true:

$$1 = P_0 + P_1 + P_2 \quad (\text{A.9})$$

Substituting equation (A.7) and (A.8) into (A.9), P_0 can be expressed as:

$$P_0 = \frac{P_D}{P_D + P_F + P_F P_D} \quad (\text{A.11})$$

The probability of a fault impacting the aircraft is the probability of being in states ‘1’ or ‘2’, which can be written as $P_{sat} = 1 - P_0$. Substituting equation (A.11) into $1 - P_0$ yields equation (1):

$$P_{sat} = \frac{P_F + P_F P_D}{P_D + P_F + P_F P_D}.$$

APPENDIX B: SATELLITE FAULT PROBABILITY USING DETECTION WITH ADVANCED ALERT

This appendix provides a derivation for equation (4). The Markov chain in Fig. 5 can be expressed in equation form as:

$$P_0(k+1) = (1 - P_F)P_0(k) + P_D P_1(k) + P_D P_2(k) \quad (B.1)$$

$$P_1(k+1) = P_F P_0(k) \quad (B.2)$$

$$P_2(k+1) = (1 - P_D)P_1(k) + (1 - P_D)P_2(k) \quad (B.3)$$

The next few steps are the same as in Appendix A. Express the steady-state form of these equations, use equation (A.9), which is still valid in this case. The following three equations are obtained:

$$P_0 = \frac{P_D}{P_F - P_F P_D} P_2 \quad (B.4)$$

$$P_1 = \frac{P_D}{1 - P_D} P_2 \quad (B.5)$$

$$P_2 = 1 - P_0 - P_1 \quad (B.6)$$

Substituting equations (B.4) and (B.5) into (B.6), and recognizing that the probability of a fault impacting the aircraft is the probability of being in state ‘2’, i.e., $P_{sat} = P_2$, we obtain equation (4):

$$P_{sat} = \frac{P_F - P_F P_D}{P_F + P_D}$$

APPENDIX C: REFERENCE STATION MEASUREMENT ERROR MODEL

This appendix describes the RS measurement error model. Sources of error affecting code and carrier phase measurements include receiver noise and multipath, troposphere, and the time-transfer process needed to synchronize the network.

We assume raw code and carrier measurement error standard deviations of 0.5 m and 0.01 m, respectively. These standard deviations are multiplied by a 2.588 factor to account for the ionosphere-free combination at L1 and L5 frequencies. A 5 min sample interval is implemented to decorrelate multipath errors. A zenith tropospheric error model with standard deviation of 0.05 m (scaled for lower elevation satellites using the tropospheric mapping function given in [3] [4]) and a time constant of two hours is also used.

In addition, RS are not time-synchronized. In response, at a given RS, we estimate the ground receiver clock bias using code and carrier measurements from all visible SVs, except for the one SV being monitored. This assumes that the other SV positions are known – but we are trying to establish true SV positions. We solve this problem iteratively, taking as initial guess the CSP navigation message (rather than the overlay), solving for RS time, then for SV position.

The measurement error covariance matrix \mathbf{V}_i in equations (16) and (21) takes all of these parameters into account. Off-diagonal components of \mathbf{V}_i account for the facts (a) that troposphere and time-transfer errors are identical for code and carrier, (b) that tropospheric error is time-correlated (it is modeled here as a first-order Gauss-Markov Process with a two hour time constant), and (c) that the time-transfer process is correlated across RS’s.

ACKNOWLEDGMENTS

The authors would like to thank the Federal Aviation Administration for sponsoring this work. The authors would also like to thank Dr. Todd Walter from Stanford University for providing explanations on potential causes for large clock errors on PRN1 and PRN24.

REFERENCES

- [1] Lee, Y. C., “Analysis of Range and Position Comparison Methods as a Means to Provide GPS Integrity in the User Receiver,” *Proc. of the 42nd Annual Meeting of The Institute of Navigation*, Seattle, WA, 1986, pp. 1-4.
- [2] Parkinson, B. W., and Axelrad, P., “Autonomous GPS Integrity Monitoring Using the Pseudorange Residual,” *NAVIGATION*, Vol. 35, No. 2, 1988, pp. 225-274.
- [3] EU-US Cooperation on Satellite Navigation, WG C-ARAIM Technical Subgroup, “ARAIM Technical Subgroup Interim Report, Issue 1.0”, 2012, available online :
<http://www.gps.gov/policy/cooperation/europe/2013/working-group-c/ARAIM-report-1.0.pdf>
http://ec.europa.eu/enterprise/newsroom/cf/getdocument.cfm?doc_id=7793

- [4] EU-US Cooperation on Satellite Navigation, WG C-ARAIM Technical Subgroup, "ARAIM Technical Subgroup Milestone 2 Report", to be published in 2015.
- [5] Blanch, J., T. Walter, P. Enge, S. Wallner, F. A. Fernandez, R. Dellago, R. Ioannides, I. F. Hernandez, B. Belabbas, A. Spletter, M. Rippl, "Critical Elements for a Multi-Constellation Advanced RAIM," *NAVIGATION*, Vol. 60, No. 1, 2013, pp. 53-69.
- [6] Global Positioning System Directorate Systems Engineering and Integration, "Interface Specification IS-GPS-200," Revision H, 2013. *available online at* <http://www.gps.gov/technical/icwg/IS-GPS-200H.pdf>
- [7] Assistant Secretary of Defense for Command, Control, Communications and Intelligence. "Global Positioning System Standard Positioning Service Performance Standard." Washington, DC, 2008. *available online at* <http://www.gps.gov/technical/ps/2008-SPS-performance-standard.pdf>
- [8] Heng, L., Gao, G., Walter, T., Enge, P., "Automated Verification of Potential GPS Signal-In-Space Anomalies Using Ground Observation Data," *Proceedings of IEEE/ION PLANS 2012*, Myrtle Beach, South Carolina, April 2012, pp. 1111-1118.
- [9] Brown, R. Grover, "A Baseline GPS RAIM Scheme and a Note on the Equivalence of Three RAIM Methods", *NAVIGATION*, Vol. 39, No. 3, Fall 1992, pp. 301-316.
- [10] van Graas, F., Farrell, J., "Baseline Fault Detection and Exclusion Algorithm," *Proceedings of the 49th Annual Meeting of The ION*, Cambridge, MA, June 1993, pp. 413-420.
- [11] Brenner, Mats, "Integrated GPS/Inertial Fault Detection Availability," *Proceedings of the 8th International Technical Meeting of the Satellite Division of The Institute of Navigation (ION GPS 1995)*, Palm Springs, CA, September 1995, pp. 1949-1958.
- [12] DeCleene, B., "Defining Pseudorange Integrity - Overbounding," *Proceedings of the 13th International Technical Meeting of the Satellite Division of The Institute of Navigation (ION GPS 2000)*, Salt Lake City, UT, September 2000, pp. 1916-1924.
- [13] Crassidis, J., and Junkins, J., *Optimal Estimation of Dynamic Systems*, Chapman & Hall/CRC, 2004.
- [14] Warren, D., and Raquet, J., "Broadcast vs. Precise GPS Ephemerides: a Historical Perspective," *GPS Solutions*, Springer Berlin / Heidelberg, Vol. 7, No. 3, 2003, pp. 151-156.
- [15] Cohenour, Curtis, van Graas, Frank, "GPS Orbit and Clock Error Distributions", *NAVIGATION, Journal of The Institute of Navigation*, Vol. 58, No. 1, Spring 2011, pp. 17-28.
- [16] Heng, L., "Safe Satellite Navigation with Multiple Constellations: Global Monitoring of GPS and GLONASS Signal-In-Space Anomalies," Ph.D. Dissertation, Stanford University, 2012.
- [17] Dow, J.M., Neilan, R. E., and Rizos, C., "The International GNSS Service in a changing landscape of Global Navigation Satellite Systems," *Journal of Geodesy*, Vol. 83, 2009, 191-198, DOI: 10.1007/s00190-008-0300-3
- [18] Walter, T., personal conversation.